Journal of Organometallic Chemistry 721-722 (2012) 148–154

Contents lists available at SciVerse ScienceDirect

Journal of Organometallic Chemistry

journal homepage: www.elsevier.com/locate/jorganchem

Experimental and computational evidence of octa- and nona-coordinated planar iron-doped boron clusters: Fe©B_8^- and Fe©B_9^-

Constantin Romanescu [a], Timur R. Galeev [b], Alina P. Sergeeva [b], Wei-Li Li [a], Lai-Sheng Wang [a,*], Alexander I. Boldyrev [b,*]

[a] Department of Chemistry, Brown University, Providence, RI 02912, USA
[b] Department of Chemistry and Biochemistry, Utah State University, 0300 Old Main Hill, Logan, UT 84322, USA

ARTICLE INFO

Article history:
Received 28 June 2012
Received in revised form
25 July 2012
Accepted 26 July 2012

We dedicated this article to 70th birthday of Professor Thomas P. Fehlner.

Keywords:
Borometallic compounds
Molecular wheels
Aromaticity
Photoelectron spectroscopy
Ab initio calculations

ABSTRACT

We report the observation of two Fe-doped boron clusters with wheel-type structures, containing an octa-coordinate (C_{8v}-Fe©B_8^-) and a nona-coordinate (D_{9h}-Fe©B_9^-) Fe atom. The clusters were produced in a laser vaporization supersonic molecular beam and characterized by combined photoelectron spectroscopy and *ab initio* studies. Chemical bonding analyses revealed that in the ground state both clusters are doubly ($\sigma + \pi$) aromatic and that the iron atom interacts with the peripheral boron ring exclusively through delocalized bonds. These findings provide further support to the design principle for metal-doped boron clusters with highly symmetric molecular wheel-type structures.

1. Introduction

The study of atomic clusters, with structures and properties intermediate between the individual entities and the bulk condensed phase, has significantly enriched our understanding of chemical bonding and the rational design of molecules with tailored physical and chemical properties [1]. Bulk boron and boranes usually have three-dimensional (3D) structures [2]. However, joint photoelectron spectroscopy and computational studies over the last decade have demonstrated that negatively charged boron clusters (B_n^-) have planar or quasi-planar structures at least up to $n = 21$ [3–13]. Neutral boron clusters were shown to become 3D at B_{20} [9], which have been corroborated by recent computational studies [14,15]. Positively charged boron clusters have been shown to become 3D at B_{16}^+ [16], while negatively charged boron clusters are still planar at B_{21}^- [13]. All planar boron clusters confirmed experimentally consist of an outer ring featuring strong two-center–two-electron (2c–2e) B–B bonds and one or more inner atoms interacting with the peripheral ring via delocalized σ and π bonding.

Two planar anionic boron clusters stand out as perfectly symmetric molecular wheel systems with unprecedented multi-center electron delocalization: B_8^{2-} (B©B_7^{2-}) and B_9^- (B©B_8^-) [4,17]. Detailed bonding analyses of the two clusters demonstrated that both species have closed shell electronic configurations and are doubly aromatic with 6 σ and 6 π delocalized electrons. The doubly aromatic character and the multi-center electron delocalization were confirmed by ring current calculations [18] and Adaptive Natural Density Partitioning (AdNDP) [19,20] analyses. Pure all-boron clusters have been proposed as novel building blocks of solid materials [21], and recently a remarkable $Ti_7Rh_4Ir_2B_8$ compound containing planar B_6 ring has been synthesized [22,23]. Fehlner and co-workers [24,25] synthesized earlier the $(Cp^*ReH_2)B_5Cl_5$ and $(Cp^*)_2B_6H_4Cl_2$ triple-decker compounds, containing the first planar B_5Cl_5 and $B_6H_4Cl_2$ structural fragments, respectively.

Numerous theoretical reports have concerned carbon-doped boron clusters featuring a carbon atom with high coordination numbers [26–30]. However, joint experimental and theoretical studies have proved that carbon avoids hyper-coordination in B_xC_y clusters [20,31–33]. One question arises: is it possible to substitute

* Corresponding authors.
E-mail addresses: Lai-Sheng_Wang@brown.edu (L.-S. Wang), a.i.boldyrev@usu.edu (A.I. Boldyrev).

0022-328X/$ – see front matter © 2012 Elsevier B.V. All rights reserved.
http://dx.doi.org/10.1016/j.jorganchem.2012.07.050

the central boron atom in the B_8^{2-} and B_9^- molecular wheels with a metal atom and therefore create metal-centered monocyclic boron clusters? We have shown previously that simple valence isoelectronic substitution of the central boron atom by aluminum in B_8^- and B_9^- lowers the symmetry of the system and gives rise to "umbrella"-type structures in AlB_7^- (C_{7v}) and AlB_8^- (C_{8v}) [34]. In these clusters, Al is bound ionically to a doubly aromatic B_7^{3-} or B_8^{2-} moiety and does not participate in delocalized bonding. Formation of ionic bonds in Al-doped boron clusters was also observed for larger AlB_n^- ($n = 9–11$) clusters [35,36]. Doping boron rings with transition metals with partially filled d-orbitals hence becomes the natural choice for creating thermodynamically stable metal-centered aromatic compounds.

Recently, we proposed a design principle for such compounds that uses the formal valence of the transition metal (x), the number of peripheral boron atoms (n), and the cluster's charge (q) to predict doubly aromatic structures ($M^{(x)}©B_n^{q-}$) and tested it for anionic, $Co©B_8^-$, $Ru©B_9^-$ [37], $Ta©B_{10}^-$, $Nb©B_{10}^-$ [38], and neutral, $Rh©B_9$ and $Ir©B_9$ [39] clusters. The design principle, derived from the bonding model of the doubly aromatic $B©B_7^{2-}$ and $B©B_8^-$ clusters [4], requires that the bonding electrons in the system, $3n + x + q$, participate in n (2c–2e) B–B peripheral bonds and 2 sets of aromatic delocalized bonds, each set fulfilling Hückel's rule for aromaticity ($4N + 2$ electrons). Geometric constraints are expected to set the minimum boron ring size (n) to 8 atoms or more, depending on the size of the dopant. When applied to Fe, the design principle predicts the following closed-shell doubly aromatic species: FeB_8^{2-}, FeB_9^-, and FeB_{10}^0. In all these clusters, the Fe atom has a formal valence of 2. Open-shell doubly aromatic systems may, also, exist for FeB_8^- and FeB_9^0, where the formal valence of Fe is 3.

Prior to this study there were no experimental reports on any Fe-doped boron clusters and there are only a few computational reports on wheel-type clusters. The most relevant works [40,41] investigated the electronic structures and geometries of a number of metal-centered boron clusters using global minimum search and DFT calculations. These studies showed that in the ground state FeB_9^- is aromatic and has a D_{9h} symmetry and that the D_{8h}-$Fe©B_8^{2-}$ wheel structure is also the global minimum on the FeB_8^{2-} potential energy surface. There have been also several other studies about the geometry optimizations and energy calculations using DFT methods for neutral and charged Fe-doped boron clusters [42–44].

In the current work, we report experimental and computational evidence demonstrating that $Fe©B_8^-$ and $Fe©B_9^-$ are doubly aromatic metal-centered borometallic compounds.

2. Experimental and computational methods

2.1. Photoelectron spectroscopy

The experiment was performed using a magnetic-bottle PES apparatus equipped with a laser vaporization cluster source that was described in detail previously [45,46]. Briefly, the iron-doped boron clusters were produced by means of laser ablation of a disk target made of isotopically enriched ^{10}B (96%), which contained ~10% ^{10}B and ~2.5% Fe by mass, balanced by Bi, which acted as a target binder and also provided the Bi^- calibrant for the photoelectron spectra. The clusters were entrained by a He carrier gas containing 5% Ar and underwent a supersonic expansion to form a collimated cluster beam. The composition and the cooling of the clusters were controlled by the time delay between the carrier gas pulse and the ablation laser [47,48]. The negatively charged clusters were extracted and analyzed with a time-of-flight mass spectrometer. The species of interest were mass-selected and decelerated before being photodetached by a pulsed laser beam at 193 nm (6.424 eV) or 266 nm (4.661 eV). Photoelectrons were collected at nearly 100% efficiency by a magnetic bottle and analyzed in a 3.5 m long electron flight tube. The electron kinetic energy resolution of the apparatus, $\Delta E/E$, was better than 2.5%, *i.e.* 25 meV for 1 eV electrons.

2.2. Computational methods

Since $Fe©B_9^-$ was already established as the global minimum of FeB_9^- in a previous theoretical report [40], we ran an extensive global minimum search only for FeB_8^-. The search was conducted using the Coalescence Kick method [49] and the UPBE0 [50,51]/LANL2DZ [52] level of theory. Low-lying isomers, within 50 kcal/mol with respect to the lowest energy isomer, were reoptimized using the aug-cc-pVTZ [53–55] basis set and the BP86 density functional [56,57], which was shown to perform slightly better than hybrid functionals for molecules containing first row transition metals [58]. Frequency calculations were performed at UBP86/aug-cc-pVTZ to ensure that all the found structures are true minima on the potential energy surface (see Fig. S1 in the Supplementary material). ROCCSD(T) [59–61]/6–311 + G(2df) [62–65]//UBP86/aug-cc-pVTZ single-point energies were calculated for low-lying isomers within 30 kcal/mol of the global minimum at the BP86 level (Fig. S1). Theoretical VDEs for FeB_8^- and FeB_9^- were calculated for the global minimum structures at the following levels of theory: U(RO)BP86/aug-cc-pVTZ, ROPBE0/aug-cc-pVTZ and ROCCSD(T)/aug-cc-pVTZ; all at the anion geometries optimized at the UBP86/aug-cc-pVTZ level of theory. The calculations were performed using Gaussian 09 [66] and Molekel 5.4.0.8 [67] was used for visualization.

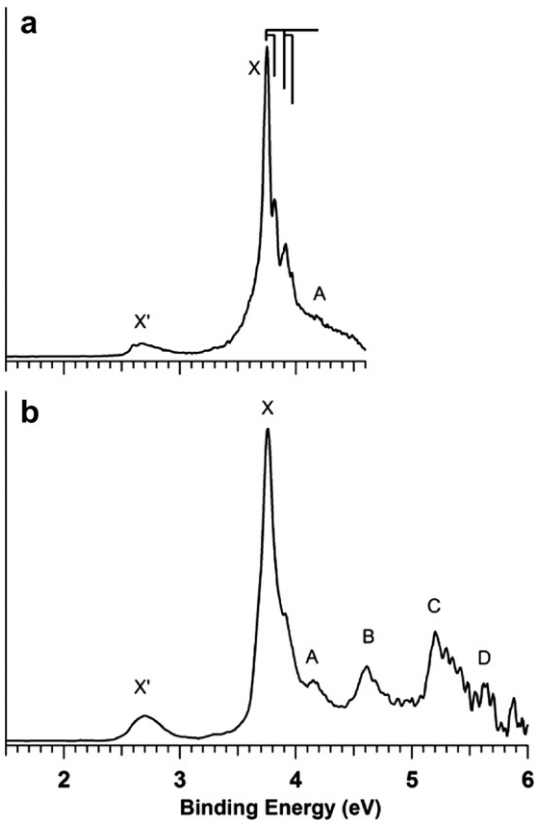

Fig. 1. Photoelectron spectra of FeB_8^- at (a) 266 nm and (b) 193 nm photodetachment wavelengths. The vertical lines indicate resolved vibrational structures.

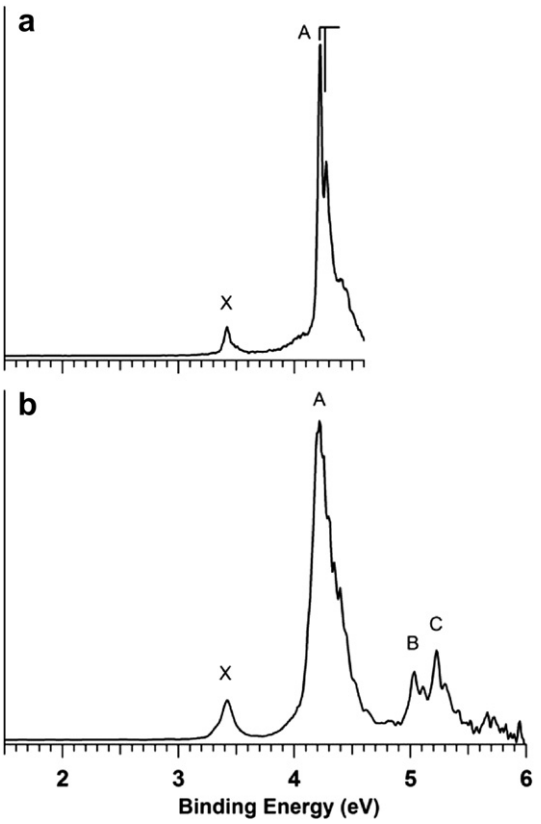

Fig. 2. Photoelectron spectra of Fe©B_9^- at (a) 266 nm and (b) 193 nm photodetachment wavelengths. The vertical lines represent resolved vibrational structures.

3. Experimental results

The photoelectron spectra of FeB_8^- and FeB_9^- are shown in Figs. 1 and 2, respectively, each at two photodetachment photon energies: 266 nm and 193 nm. The detachment features are labeled with letters and the measured vertical detachment energies (VDE) are given in Table 1, where they are compared with theoretical calculations at various levels of theory (*vide infra*). Commonly, the peak marked as X represents the transition between the ground electronic states of the anion and the neutral species, while the higher binding energy peaks (A, B…) denote transitions to excited electronic states of the neutral cluster.

3.1. FeB_8^-

The 266 nm spectrum of FeB_8^- (Fig. 1a) displays a broad and weak low binding energy band (X′), an intense vibrationally resolved band (X), and a weak band A. As will be shown below, the first band (X′) represents probably a transition from a higher energy isomer. The strong feature in the 266 nm spectrum (X) corresponds to the transition from the ground state of FeB_8^- to that of its neutral with a VDE value of 3.75 eV and a partially resolved vibrational progression. Two vibrational modes are tentatively assigned with average spacings of 510 ± 50 cm^{-1} and 1300 ± 100 cm^{-1}, respectively. Since this band does not have a sharp rise, it is likely that there may be unresolved low frequency vibrational excitations associated with each resolved peak. The adiabatic detachment energy (ADE) of band X is evaluated to be 3.65 eV. The third weak feature, A, with a VDE of 4.15 eV, was not well resolved at 266 nm, but it is better defined in the 193 nm spectrum (Fig. 1b). At the high binding energy side, we observed three additional bands B–D with VDEs of 4.60, 5.21, and 5.60 eV, respectively. All the spectral features of FeB_8^- are broad, suggesting that there are significant geometry changes between FeB_8^- and its neutral states.

3.2. FeB_9^-

The 266 nm photoelectron spectrum of FeB_9^- (Fig. 2a) displays two detachment bands: X and A. The first band, X, is weak with a vertical detachment energy (VDE) value of 3.42 eV and does not show any resolved vibrational structure. The ADE is 3.38 (3) eV. The second band, A, is intense and has a VDE value of 4.22 eV. The A band has a sharp rise and shows a short vibrational progression with an average spacing of 440 ± 40 cm^{-1}. We assign the most intense peak of the A band

Table 1
Theoretically calculated VDEs for the Fe©B_8^- (C_{8v}, $^2A_1$) and Fe©B_9^- (D_{9h}, $^1A_1'$) clusters. All energies are in eV.

Feature	VDE (exp)[a]	Final state and electronic configuration	VDE (theoretical)		
			UBP86[b]	ROPBE0[c]	ROCCSD(T)[d]
FeB_8^- (C_{8v}, $^2A_1$)					
X	3.75 (3)	$^3E_1$ … $2e_1^4\,2a_1^2\,3a_1^2\,2e_2^4\,3e_1^3\,4a_1^1$	3.62 (0.80)	3.71	3.84 (1.41)
A	4.15 (4)	$^3E_2$ … $2e_1^4\,2a_1^2\,3a_1^2\,2e_2^3\,3e_1^4\,4a_1^1$	4.17 (2.04)	3.81	4.06 (1.34)
B	4.60 (5)	$^1A_1$ … $2e_1^4\,2a_1^2\,3a_1^2\,2e_2^4\,3e_1^4\,4a_1^0$	4.58 (0.00)	4.79	5.06 (1.68)[f]
C	5.21 (5)	$^3A_1$ … $2e_1^4\,2a_1^2\,3a_1^1\,2e_2^4\,3e_1^4\,4a_1^1$	5.17 (2.03)	5.16	5.30 (1.33)
		$^3E_1$ … $2e_1^3\,2a_1^2\,3a_1^2\,2e_2^4\,3e_1^4\,4a_1^1$	5.35 (2.07)	[e]	5.24 (1.36)
D	5.6 (1)	$^3A_1$ … $2e_1^4\,2a_1^1\,3a_1^2\,2e_2^4\,3e_1^4\,4a_1^1$	5.60 (2.08)	5.78	5.66 (1.37)
Fe©B_9^- (D_{9h}, $^1A_1'$)					
X	3.42 (3)	$^2A_1'$ … $1a_2''^2\,1e_1''^4\,2e_2'^4\,2e_1'^4\,3a_1'^1$	3.58[g]	3.40	[h]
A	4.22 (3)	$^2E_1'$ … $1a_2''^2\,1e_1''^4\,2e_2'^4\,2e_1'^3\,3a_1'^2$	4.05 (0.77)	4.19	[h]
		$^2E_2'$ … $1a_2''^2\,1e_1''^4\,2e_2'^3\,2e_1'^4\,3a_1'^2$	4.42[g]	4.10	[h]
B	5.03 (4)	$^2E_1''$ … $1a_2''^2\,1e_1''^3\,2e_2'^4\,2e_1'^4\,3a_1'^2$	5.08 (0.80)	4.69	[h]
C	5.23 (4)	$^2A_2''$ … $1a_2''^1\,1e_1''^4\,2e_2'^4\,2e_1'^4\,3a_1'^2$	5.26[g]	5.26	[h]

[a] Numbers in parentheses represent the uncertainty in the last digit.
[b] VDEs were calculated at UBP86/aug-cc-pVTZ. The values of $\langle S^2\rangle$ are given in parentheses following the computed VDE values.
[c] VDEs were calculated at ROPBE0/aug-cc-pVTZ//UBP86/aug-cc-pVTZ.
[d] VDEs were calculated at ROCCSD(T)/6–311 + G(2df)//UBP86/aug-cc-pVTZ. The NORM values are given in parentheses following the computed VDE values.
[e] We couldn't achieve convergence for this particular state.
[f] The validity of this VDE value is questionable due to the high NORM value.
[g] In these cases high spin contamination of the final neutral states was encountered (with $\langle S^2\rangle$ higher than 0.8). Therefore the VDEs were calculated at ROBP86/aug-cc-pVTZ.
[h] The calculations of the neutral states of FeB_9 resulted in very high NORM values ranging from 1.54 to 2.67. Due to inaccuracy of the computed values we are not presenting those in the table.

to the 0–0 vibrational transition, as the measured ADE and VDE values are equal. At 193 nm (Fig. 2b), two more features are identified, B and C, with VDE values of 5.03 and 5.23 eV. No discernable spectral features were observed beyond 6 eV. All detachment transitions were relatively sharp, suggesting that there are only minor geometry changes between the anion and the neutral states.

4. Theoretical results

The global minimum structures of FeB_8^- and FeB_9^- are presented in Fig. 3. FeB_9^- has a perfectly symmetric planar D_{9h} structure whereas the FeB_8^- species is a slightly distorted wheel-type structure of C_{8v} symmetry. The extent of distortion could be evaluated by noting that the largest B–Fe–B angle in the C_{8v} structure is 160.0°. The valence canonical molecular orbitals of the anionic species are presented in Fig. 4. The global minimum of FeB_8^- has one unpaired electron in the singly occupied molecular orbital (HOMO, $4a_1$) giving rise to the lowest doublet $^2A_1$ state of the C_{8v} structure (Fig. 4a) while all the molecular orbitals of FeB_9^- are doubly occupied rendering the closed-shell $^1A_1'$ state of the species (Fig. 4b). The diagrams of highest occupied and lowest unoccupied orbitals of both FeB_8^- and FeB_9^-, as well as the orbital energies at ROBP86/aug-cc-pVTZ are given in Fig. 4c.

4.1. FeB_8^-

We performed an unbiased global minimum search for FeB_8^- using the Coalescence Kick method [49]. All of the structures found in this search within 50 kcal/mol at PBE0/LANL2DZ were further reoptimized at UBP86/aug-cc-pVTZ following the energy gradient to the closest minima (Fig. S1 in the Supplementary material). The C_{8v} structure of FeB_8^- (Fig. 3a) was found to be the lowest energy isomer with all the other structures lying higher than 20 kcal/mol with respect to the global minimum at UBP86/aug-cc-pVTZ. The subsequent single point calculations at ROCCSD(T)/6-311 + G(2df)//UBP86/aug-cc-pVTZ for all the low-lying isomers of FeB_8^-, identified within 30 kcal/mol at UBP86/aug-cc-pVTZ, confirmed that the C_{8v}-FeB_8^- structure is the true global minimum on the potential energy surface of FeB_8^- (Fig. S1). It should be pointed out that we encountered a very high value of Norm(A) = 2.05 (Norm(A) gives a measure of the correlation correction to the wavefunction; the coefficient of the HF configuration is 1) in our calculation of the ROCCSD(T) energy for the second lowest isomer of FeB_8^- (slightly distorted octa-coordinate wheel-type structure in a quartet state, isomer I.2, Fig. S1). Therefore, the relative energy of 27.1 kcal/mol at the ROCCSD(T) level for the second lowest isomer of FeB_8^- is highly questionable. It suggests that multi-configurational calculations are needed for this high spin isomer, which are beyond the scope of the current work.

We calculated the VDEs for the global minimum at UBP86, ROPBE0 and ROCCSD(T) levels (see Table 1) and for the second lowest isomer of FeB_8^- at UBP86 (see Table S1 in the Supplementary material) and found a good agreement between the experimental features X, A, B, C, D and transitions in the C_{8v} structure of FeB_8^-, whereas the first VDE of the second lowest isomer of FeB_8^- agrees well with the broad X′ band in the lower binding energy region.

4.2. FeB_9^-

The lowest planar wheel-type structure featuring a nona-coordinate iron (Fig. 3b) was identified in the work by Ito et al. in stochastic searches of both singlet and triplet potential energy surfaces of FeB_9^- [40]. All other structures were found to lie higher in energy [40]. Therefore, in the current study we did not perform a global minimum search for FeB_9^-. Instead we reoptimized the D_{9h} global minimum structure of FeB_9^- at UBP86/aug-cc-pVTZ, further calculated its VDEs at the U(RO)BP86, ROPBE0, and ROCCSD(T) levels, and compared the VDEs with the experimental data to confirm the calculated structure. All the calculated VDE values were found to be in good agreement with the experimental values.

5. Comparison of experimental and theoretical results

5.1. FeB_8^-

The unbiased search for the lowest structure of FeB_8^- revealed that the global minimum structure is an octa-coordinate wheel with the central Fe atom slightly shifted out of the boron ring plane (~0.2 Å) in the C_{8v}-Fe©B_8^- structure.

The ground state detachment transition is from the removal of an electron from the doubly degenerate $3e_1$ orbital, corresponding to the X band at 3.75 eV. This transition results in a final triplet $^3E_1$ state and the calculated VDE was found to be in good agreement with the experimental value: 3.62 eV at UBP86, 3.71 eV at ROPBE0, and 3.84 eV at ROCCSD(T). As a result of the electron removal from a doubly degenerate orbital, the geometry of the neutral FeB_8 cluster undergoes a small Jahn-Teller distortion leading to a lower C_{2v} symmetry (see Fig. S2 in the Supplementary material). The geometry change was, also, reflected by the observation of the two vibrational modes of FeB_8 that are responsible for the C_{8v} to C_{2v} distortion. The experimental values, 510 (50) cm^{-1} and 1300 (100) cm^{-1}, are indeed in good agreement with the UBP86 values: 516 cm^{-1} and 1286 cm^{-1}, respectively. The A band comes from the removal of an electron from the $2e_2$ orbital, resulting in the triplet $^3E_2$ excited state of the neutral species. The B band corresponds to electron detachment from the $4a_1$ orbital. All of the other transitions are explained as electron detachments from the $3a_1$, $2a_1$, and $2e_1$ orbitals with final triplet states. All of the VDE values calculated for the photodetachment transitions are in good agreement with the experimentally measured values (Table 1) with the exception of the transition marked as X′ in Fig. 2.

This transition could be assigned to photodetachment from a higher energy isomer I.2 (Fig. S1 and Table S1 in the Supplementary material). The presence of a similar low binding energy peak was previously observed for the Co©B_8^- cluster [37] and explained as contribution from a higher spin (triplet) isomer. Isomer I.2 was the only low-energy isomer for which we could not accurately evaluate the relative energy at the ROCCSD(T) level due to a high NORM value (2.05) in our calculation. Therefore, we think it could actually be closer in energy to the global minimum than the predicted value of 27.1 kcal/mol. This isomer has an octa-coordinate

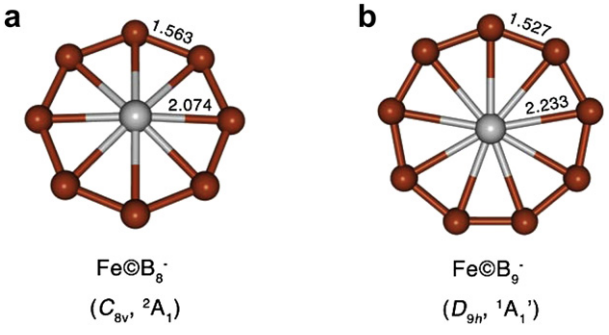

Fig. 3. Global minima of (a) Fe©B_8^- and (b) Fe©B_9^-. Geometries are optimized at the BP86/aug-cc-pVTZ level. Bond lengths are given in Å.

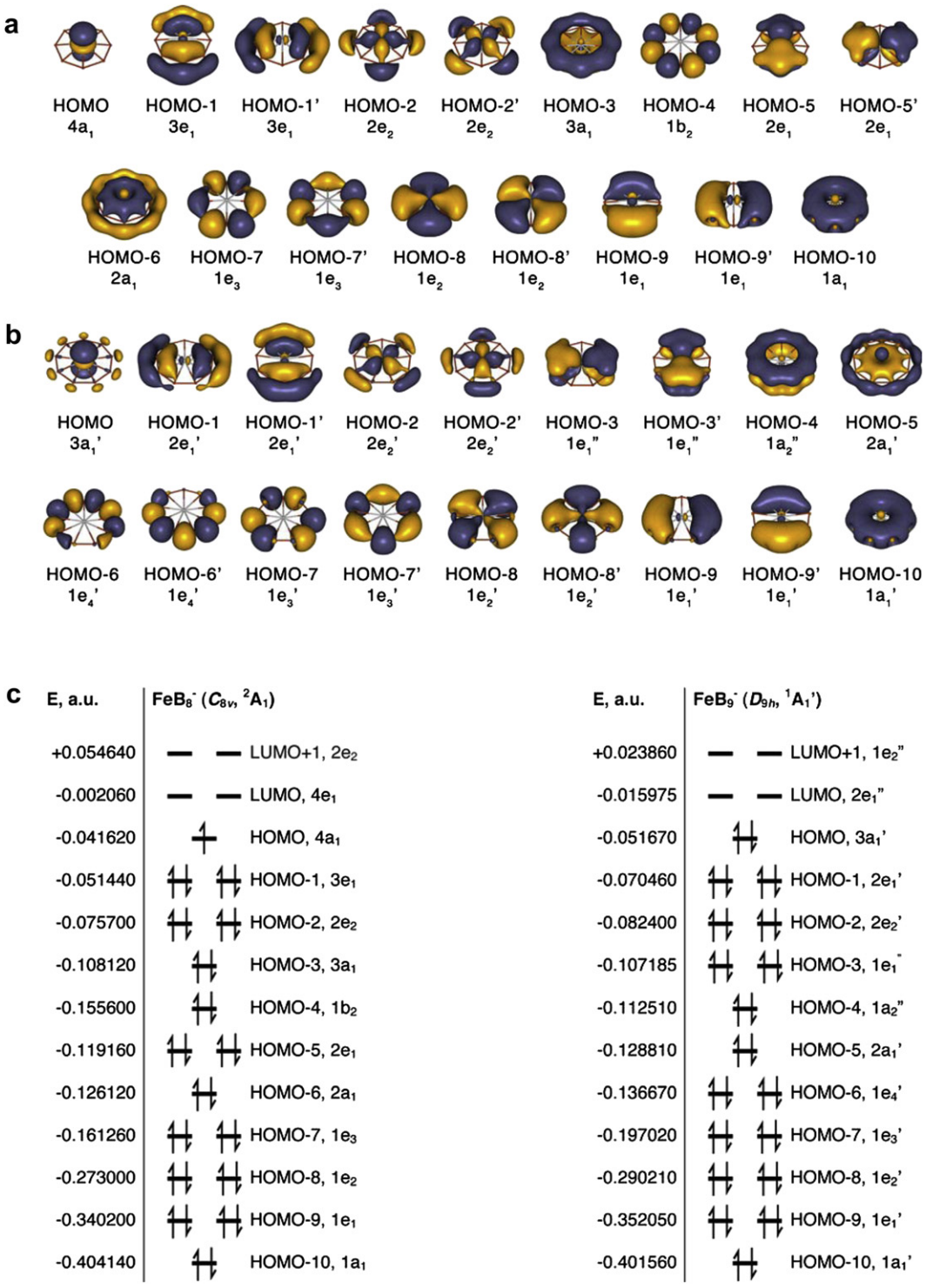

Fig. 4. The valence canonical molecular orbitals of Fe©B_8^- (a) and Fe©B_9^- (b) and their orbital energies (c) at the ROBP86/aug-cc-pVTZ level.

distorted wheel-type structure in the lowest quartet $^4A_1$ state. The detachment from a singly occupied HOMO ($5b_1$) occurs at a VDE of 2.59 eV at UBP86, which is in good agreement with the X′ band. We have also calculated VDEs of the lowest transitions for isomer I.3 and isomer I.4 to be 2.67 eV and 2.53 eV, respectively. We could not exclude contributions of these isomers to the X′ band, though we believe that they should be minor because these isomers are quite high in energy. The highly multi-configurational character of the electronic states of the open shell FeB_8^- makes *ab initio* calculations at higher levels of theory extremely challenging. The good agreement between the theoretical VDEs and the experimental data lends support for the slightly distorted C_{8v} molecular wheel structure as the global minimum for FeB_8^-. Thus, we found the global minimum of Fe©B_8^- to possess an octa-coordinate iron atom in which Fe is slightly shifted out of the molecular plane formed by the outer boron ring (Fig. 3a).

The optimized geometries of the dianionic, anionic, and neutral $FeB_8^{2-/1-/0}$ cluster at BP86/aug-cc-pVTZ are compared in Figure S2. It

can be clearly seen that the peripheral B–B distance becomes somewhat shorter (1.572 Å for $Fe©B_8^{2-}$; 1.563 Å for $Fe©B_8^-$; 1.548 Å for $Fe©B_8$) while the central iron atom gets more and more out of plane as we gradually remove two electrons from the octa-coordinate $Fe©B_8^{2-}$ species introduced by Pu et al. [41].

The canonical molecular orbitals (CMO) of the open-shell global minimum of $Fe©B_8^-$ are presented in Fig. 4a. We expect that the 33 valence electrons of $Fe©B_8^-$ could form the following bonds and lone pairs: 1) three π delocalized bonds making this cluster π aromatic; 2) three σ delocalized bonds making this cluster σ aromatic; 3) two lone pairs of d-type participating in a minor covalent bonding with the peripheral boron ring; 4) a singly occupied 1c–2e bond of d_z2-type localized on the central atom; 5) eight 2c–2e peripheral B–B σ bonds. The double aromaticity of the FeB_8^- global minimum explains its stability and presence in the photoelectron spectrum.

5.2. FeB_9^-

The previously reported global minima stochastic searches revealed that the wheel-type structure is the lowest energy isomer of FeB_9^- [40]. The first low-lying isomer (C_s) was shown to be 14.9 kcal/mol higher in energy at the BP86/TZVPP level of theory [40] and, therefore, we expect that only the wheel structure should contribute to the photoelectron signal in the photodetachment spectra.

The AdNDP analysis reported previously [20] showed that the system is doubly aromatic (σ + π) and that Fe acts as valence 2 element. The six 3d electrons of Fe are localized as lone pairs (d_z2, d_x2_y2, d_{xy}), however, there is some bonding interaction between the peripheral boron ring and the d_x2_y2 and d_{xy} electrons (occupation number, ON = 1.80|e|). Even though this system is valence isoelectronic to $Ru©B_9^-$ we note that there are differences between their MO patterns [37]. In the case of $Ru©B_9^-$ the HOMO (3a′) is essentially the $4d_z2$ atomic orbital of Ru and does not contribute to bonding (ON = 2.00|e|). Removal of a single electron from the $4d_z2$ HOMO does not lead to a large geometry change and causes only a slight out-of-plane displacement of the Ru atom. Its HOMO-1 ($2e_1'$) consists of a set of doubly degenerate σ bonding orbitals and Jahn-Teller geometric distortions are expected for the electron detachment.

The experimental spectra show that the lowest binding energy transition in $Fe©B_9^-$ is relatively sharp and has no vibrationally resolved features, suggesting that this transition should involve the removal of one electron from a non-bonding orbital. This observation was confirmed by our DFT energy calculations: the first detachment channel corresponds to the removal of an electron from the $3a_1'$ HOMO similar to the HOMO of $Ru©B_9^-$ (Fig. 3) to result in the $^2A_1'$ ground state for the neutral species (Table 1). Furthermore, the geometry optimization of the neutral cluster starting from the wheel structure indicates that the D_{9h}-$Fe©B_9$ is at least a minimum on the potential energy surface of FeB_9. The minimal change in the geometry of the $Fe©B_9^-$ upon one electron photodetachment is consistent with our previous observations on the $Ru©B_9^-$ cluster [37]. In the latter case, the Ru atom was found to be slightly too large to fit inside a neutral B_9 ring and was pushed outside the ring and formed a highly symmetric C_{9v} symmetry structure. The theoretical first VDE, computed at BP86 (3.58 eV) or at PBE0 (3.40 eV), is in good agreement with the experimental feature X at 3.42 eV (Table 1). The next four photodetachment transitions occur from HOMO-1, HOMO-2, HOMO-3, and HOMO-4. The calculated VDEs for these transitions also show good agreement with the experimental data, confirming that the Fe-centered wheel structure is the global minimum of FeB_9^- [20,40].

The stability of FeB_9^- was previously attributed to its doubly aromatic character [40]. We present the canonical molecular orbitals of $Fe©B_9^-$ (Fig. 4b), which are also reported in Ref. [40]. The MOs show that this species is indeed 1) π aromatic with six delocalized π electrons (HOMO-3, HOMO-3′, and HOMO-4) satisfying the $4N + 2$ rule for π-aromaticity; 2) σ aromatic with six delocalized σ electrons (HOMO-1, HOMO-1′, and HOMO-5) satisfying the $4N + 2$ rule for σ aromaticity. The HOMO is a completely non-bonding lone pair of $3d_z2$-type centered on the Fe atom, whereas HOMO-2 and HOMO-2′ can be viewed as mainly composed of Fe 3d-type lone pairs with some minor contributions to electron density from the peripheral boron atoms. The remaining nine valence canonical molecular orbitals (HOMO-6, HOMO-6′, HOMO-7, HOMO-7′, HOMO-8, HOMO-8′, HOMO-9, HOMO-9′, and HOMO-10) are responsible for the bonding of the peripheral boron atoms with each other. Therefore, the stability of the $Fe©B_9^-$ structure was thoroughly substantiated [20,40], in agreement with our design principle.

While a ten-membered boron ring with a deca-coordinated Fe atom may exist as FeB_{10}, we believe that a 3d transition metal is too small to stabilize B_{10} ring, as we demonstrated for VB_{10}^- [68].

6. Conclusions

Joint photoelectron spectroscopy and *ab initio* studies of two Fe-doped boron clusters, FeB_8^- and FeB_9^-, have established that both clusters are doubly aromatic possessing octa- and nona-coordinate iron atom, respectively, conforming with our design principle for transition-metal-centered $M©B_n$ type molecular wheels. These novel planar metal-boron species constitute a new class of borometallic compounds and may be viable for condensed phase syntheses.

Acknowledgments

This work was supported by the NSF (DMR-0904034 to L.S.W. and CHE-1057746 to A.I.B.). Computer times from the Centers for High Performance Computing at the University of Utah and Utah State University are gratefully acknowledged.

Appendix A. Supplementary material

Supplementary material associated with this article can be found, in the online version, at http://dx.doi.org/10.1016/j.jorganchem.2012.07.050.

References

[1] T.P. Fehlner, J.-F. Halet, J.-Y. Saillard, Molecular Clusters: a Bridge to Solid-State Chemistry, Cambridge University Press, Cambridge, UK, 2007.
[2] F.A. Cotton, G. Wilkinson, C.A. Murillo, M. Bochmann, Advanced Inorg. Chem., sixth ed. Wiley-Interscience, New York, 1999.
[3] H.J. Zhai, L.S. Wang, A.N. Alexandrova, A.I. Boldyrev, J. Chem. Phys. 117 (2002) 7917.
[4] H.J. Zhai, A.N. Alexandrova, K.A. Birch, A.I. Boldyrev, L.S. Wang, Angew. Chem. Int. Ed. 42 (2003) 6004.
[5] H.J. Zhai, B. Kiran, J. Li, L.S. Wang, Nat. Mater. 2 (2003) 827.
[6] H.J. Zhai, L.S. Wang, A.N. Alexandrova, A.I. Boldyrev, V.G. Zakrzewski, J. Phys. Chem. A 107 (2003) 9319.
[7] A.N. Alexandrova, A.I. Boldyrev, H.J. Zhai, L.S. Wang, E. Steiner, P.W. Fowler, J. Phys. Chem. A 107 (2003) 1359.
[8] A.N. Alexandrova, A.I. Boldyrev, H.J. Zhai, L.S. Wang, J. Phys. Chem. A 108 (2004) 3509.
[9] B. Kiran, S. Bulusu, H.J. Zhai, S. Yoo, X.C. Zeng, L.S. Wang, Proc. Natl. Acad. Sci. U. S. A. 102 (2005) 961.
[10] A.P. Sergeeva, D.Y. Zubarev, H.J. Zhai, A.I. Boldyrev, L.S. Wang, J. Am. Chem. Soc. 130 (2008) 7244.
[11] W. Huang, A.P. Sergeeva, H.J. Zhai, B.B. Averkiev, L.S. Wang, A.I. Boldyrev, Nat. Chem. 2 (2010) 202.

[12] A.P. Sergeeva, B.B. Averkiev, H.J. Zhai, A.I. Boldyrev, L.S. Wang, J. Chem. Phys. 134 (2011) 224304.
[13] Z.A. Piazza, W.L. Li, C. Romanescu, A.P. Sergeeva, L.S. Wang, A.I. Boldyrev, J. Chem. Phys. 136 (2012) 104310.
[14] T.B. Tai, N.M. Tam, M.T. Nguyen, Chem. Phys. Lett. 530 (2012) 71.
[15] F. Li, P. Jin, D.e. Jiang, L. Wang, S.B. Zhang, J. Zhao, Z. Chen, J. Chem. Phys. 136 (2012) 074302.
[16] E. Oger, N.R.M. Crawford, R. Kelting, P. Weis, M.M. Kappes, R. Ahlrichs, Angew. Chem. Int. Ed. 46 (2007) 8503.
[17] A.N. Alexandrova, H.J. Zhai, L.S. Wang, A.I. Boldyrev, Inorg. Chem. 43 (2004) 3552.
[18] P.W. Fowler, B.R. Gray, Inorg. Chem. 46 (2007) 2892.
[19] D.Y. Zubarev, A.I. Boldyrev, Phys. Chem. Chem. Phys. 10 (2008) 5207.
[20] B.B. Averkiev, L.M. Wang, W. Huang, L.S. Wang, A.I. Boldyrev, Phys. Chem. Chem. Phys. 11 (2009) 9840.
[21] A.N. Alexandrova, A.I. Boldyrev, H.J. Zhai, L.S. Wang, Coord. Chem. Rev. 250 (2006) 2811.
[22] B.P.T. Fokwa, M. Hermus, Angew. Chem. Int. Ed. 51 (2012) 1702.
[23] V.L. Deringer, C. Goerens, M. Esters, R. Dronskowski, B.P.T. Fokwa, Inorg. Chem. 51 (2012) 5677.
[24] S. Ghosh, A.M. Beatty, T.P. Fehlner, J. Am. Chem. Soc. 123 (2001) 9188.
[25] B. Le Guennic, H. Jiao, S. Kahlal, J.Y. Saillard, J.F. Halet, S. Ghosh, M. Shang, A.M. Beatty, A.L. Rheingold, T.P. Fehlner, J. Am. Chem. Soc. 126 (2004) 3203.
[26] K. Exner, P.v.R. Schleyer, Science 290 (2000) 1937.
[27] Z.X. Wang, P.v.R. Schleyer, Science 292 (2001) 2465.
[28] S. Erhardt, G. Frenking, Z.F. Chen, P.v.R. Schleyer, Angew. Chem. Int. Ed. 44 (2005) 1078.
[29] R. Islas, T. Heine, K. Ito, P.v.R. Schleyer, G. Merino, J. Am. Chem. Soc. 129 (2007) 14767.
[30] K. Ito, Z.F. Chen, C. Corminboeuf, C.S. Wannere, X.H. Zhang, Q.S. Li, P.v.R. Schleyer, J. Am. Chem. Soc. 129 (2007) 1510.
[31] L.M. Wang, W. Huang, B.B. Averkiev, A.I. Boldyrev, L.S. Wang, Angew. Chem. Int. Ed. 46 (2007) 4550.
[32] B.B. Averkiev, D.Y. Zubarev, L.M. Wang, W. Huang, L.S. Wang, A.I. Boldyrev, J. Am. Chem. Soc. 130 (2008) 9248.
[33] T.R. Galeev, A.S. Ivanov, C. Romanescu, W.L. Li, K.V. Bozhenko, L.S. Wang, A.I. Boldyrev, Phys. Chem. Chem. Phys. 13 (2011) 8805.
[34] T.R. Galeev, C. Romanescu, W.L. Li, L.S. Wang, A.I. Boldyrev, J. Chem. Phys. 135 (2011) 104301.
[35] W.L. Li, C. Romanescu, T.R. Galeev, L.S. Wang, A.I. Boldyrev, J. Phys. Chem. A 115 (2011) 10391.
[36] C. Romanescu, A.P. Sergeeva, W.L. Li, A.I. Boldyrev, L.S. Wang, J. Am. Chem. Soc. 133 (2011) 8646.
[37] C. Romanescu, T.R. Galeev, W.L. Li, A.I. Boldyrev, L.S. Wang, Angew. Chem. Int. Ed. 50 (2011) 9334.
[38] T.R. Galeev, C. Romanescu, W.L. Li, L.S. Wang, A.I. Boldyrev, Angew. Chem. Int. Ed. 51 (2012) 2101.
[39] W.L. Li, C. Romanescu, T.R. Galeev, Z.A. Piazza, A.I. Boldyrev, L.S. Wang, J. Am. Chem. Soc. 134 (2012) 165.
[40] K. Ito, Z. Pu, Q.S. Li, P.v.R. Schleyer, Inorg. Chem. 47 (2008) 10906.
[41] Z.F. Pu, K. Ito, P.v.R. Schleyer, Q.S. Li, Inorg. Chem. 48 (2009) 10679.
[42] Q.O. Luo, Sci. China Ser. B – Chem. 51 (2008) 607.
[43] Q.Y. Wu, Y.P. Tang, X.H. Zhang, Sci. China Ser. B – Chem. 52 (2009) 288.
[44] Z. Yang, S.J. Xiong, J. Chem. Phys. 128 (2008) 184310.
[45] L.S. Wang, H.S. Cheng, J.W. Fan, J. Chem. Phys. 102 (1995) 9480.
[46] L.S. Wang, H. Wu, in: M.A. Duncan (Ed.), Advances in Metal and Semiconductor Clusters, JAI Press, Greenwich, CT, 1998, pp. 299–343.
[47] J. Akola, M. Manninen, H. Hakkinen, U. Landman, X. Li, L.S. Wang, Phys. Rev. B 60 (1999) 11297.
[48] L.S. Wang, X. Li, in: P. Jena, S.N. Khanna, B.K. Rao (Eds.), Proc. Int. Symp. on Clusters and Nanostructure Interfaces, World Scientific, River Edge, New Jersey, 2000, pp. 293–300.
[49] B.B. Averkiev, Ph.D. thesis, Utah State University, Logan, UT, USA, 2009.
[50] C. Adamo, V. Barone, J. Chem. Phys. 110 (1999) 6158.
[51] J.P. Perdew, K. Burke, M. Ernzerhof, Phys. Rev. Lett. 77 (1996) 3865.
[52] P.J. Hay, W.R. Wadt, J. Chem. Phys. 82 (1985) 299.
[53] T.H. Dunning, J. Chem. Phys. 90 (1989) 1007.
[54] R.A. Kendall, T.H. Dunning, R.J. Harrison, J. Chem. Phys. 96 (1992) 6796.
[55] N.B. Balabanov, K.A. Peterson, J. Chem. Phys. 123 (2005) 064107.
[56] A.D. Becke, Phys. Rev. A 38 (1988) 3098.
[57] J.P. Perdew, Phys. Rev. B 33 (1986) 8822.
[58] K.P. Jensen, B.O. Roos, U. Ryde, J. Chem. Phys. 126 (2007) 014103.
[59] J. Cizek, Adv. Chem. Phys. 14 (1969) 35.
[60] G.D. Purvis, R.J. Bartlett, J. Chem. Phys. 76 (1982) 1910.
[61] K. Raghavachari, G.W. Trucks, J.A. Pople, M. Head-Gordon, Chem. Phys. Lett. 157 (1989) 479.
[62] M.S. Gordon, J.S. Binkley, J.A. Pople, W.J. Pietro, W.J. Hehre, J. Am. Chem. Soc. 104 (1982) 2797.
[63] A.D. McLean, G.S. Chandler, J. Chem. Phys. 72 (1980) 5639.
[64] W.J. Pietro, M.M. Francl, W.J. Hehre, D.J. Defrees, J.A. Pople, J.S. Binkley, J. Am. Chem. Soc. 104 (1982) 5039.
[65] T. Clark, J. Chandrasekhar, G.W. Spitznagel, P.v.R. Schleyer, J. Comput. Chem. 4 (1983) 294.
[66] M.J. Frisch, G.W. Trucks, H.B. Schlegel, G.E. Scuseria, M.A. Robb, J.R. Cheeseman, G. Scalmani, V. Barone, B. Mennucci, G.A. Petersson, H. Nakatsuji, M. Caricato, X. Li, H.P. Hratchian, A.F. Izmaylov, G.Z.J. Bloino, J.L. Sonnenberg, M. Hada, M. Ehara, K. Toyota, R. Fukuda, J. Hasegawa, M. Ishida, T. Nakajima, Y. Honda, O. Kitao, H. Nakai, T. Vreven, J.A. Montgomery, J.E. Peralta Jr., F. Ogliaro, M. Bearpark, J.J. Heyd, E. Brothers, K.N. Kudin, V.N. Staroverov, R. Kobayashi, J. Normand, K. Raghavachari, A. Rendell, J.C. Burant, S.S. Iyengar, M.C.J. Tomasi, N. Rega, J.M. Millam, M. Klene, J.E. Knox, J.B. Cross, V. Bakken, C. Adamo, J. Jaramillo, R. Gomperts, R.E. Stratmann, O. Yazyev, A.J. Austin, R. Cammi, C. Pomelli, J.W. Ochterski, R.L. Martin, K. Morokuma, V.G. Zakrzewski, G.A. Voth, P. Salvador, J.J. Dannenberg, S. Dapprich, A.D. Daniels, Ö Farkas, J.B. Foresman, J.V. Ortiz, J. Cioslowski, D.J. Fox, GAUSSIAN 09, Rev. C.02, Gaussian Inc., Wallingford, CT, 2009.
[67] U. Varetto, Molekel 5.4.0.8, Swiss National Supercomputing Centre, Manno (Switzerland), 2009.
[68] W.L. Li, C. Romanescu, Z.A. Piazza, L.S. Wang, Phys. Chem. Chem. Phys., in press.